

Conformational and Electronic Consequences in Crafting Extended, π -Conjugated, Light-Harvesting Macrocycles

Leigh J. K. Boerner, Shivnath Mazumder, Maren Pink, Mu-Hyun Baik,* and Jeffrey M. Zaleski*[a]

Abstract: The synthesis of a new series of free-base, Ni^{II} and Zn^{II} 2,3,12,13-tetra(ethynyl)-5,10,15,20-tetraphenyl porphyrins is described. Upon heating, two of the four ethynyl moieties undergo Bergman cyclization to afford the monocyclized 2,3-diethynyl-5,20-diphenylpiceno[10,11,12,13,14,15-*ijklmn*]porphyrin in 30%, 10%, and trace yields, respectively. The structures of all products were investigated by using quantum chemical calculations and the free-base analogue was isolated and crystallized; all compounds show significant deviation from the idealized planar structure. No fully-cyclized bispiceno[20,1,2,3,4,5,10,11,12,13,14,15-*fg hij*]por-

phyrin was isolated from the reaction mixture. To understand why only two of the four ethynyl groups undergo Bergman cyclization, the reaction coordinates were examined by using DFT at the PWPW91/cc-pVTZ(-f) level coupled to a continuum solvation model. The barrier to cyclization of the second pair of ethynyl groups was found to be 5.5 kcal mol⁻¹ higher than the first, suggesting a negative cooperative effect and significantly slower rate for the

second cyclization. Cyclization reactions for model porphyrin-enediynes with ethene- and H-functionality substitutions at the *meso*-phenyl rings were also examined, and found to have a similar barrier to diradical formation for the second cyclization event as for the first in these highly planar molecules. By enforcing an artificial 30° cant in two of the pyrrole rings of the porphyrin, the second barrier was increased by 2 kcal mol⁻¹ in the ethene model system; this suggests that the disruption of the π conjugation of the extended porphyrin structure is the cause of the increased barrier to the second cyclization event.

Keywords: aromaticity • computational chemistry • cyclization • fused-ring systems • porphyrinoids

Introduction

Extended aromatic conjugation in macrocyclic structures plays a prominent role in light-harvesting events in photosynthesis, optical generation of singlet O₂ in photodynamic therapy,^[1] molecular wires,^[2] and photoinduced energy or charge transport in dye-sensitized, solar-energy materials.^[3] In addition to their optical significance, ground-state electronic properties, such as redox potentials, are critical to metalloenzyme function and the stabilization of high oxidation states in key intermediates (e.g., cytochrome P450). The consequences of extended conjugation can also dictate chemical transformations at the macrocycle periphery due to the modulation of net electro- or nucleophilicity at fringe functionalities.^[4] Such transformations can also be affected by structural conformations caused by steric strain, which in

turn translates into perturbations in the electronic system.^[5] Thus, effective construction of aromatic molecules with extended conjugation requires a subtle balance of appropriate geometric conformation fused to electronic stability derived from increased delocalization. Proper harnessing of these properties can result in large, rigid, exocyclic, aromatic architectures that possess long-wavelength absorption, high transmission efficiencies, and large emission quantum yields.^[4c,6]

The most straightforward and widely employed strategy for preparation of these π -extended, light-harvesting motifs involves fusion of a rigid, aromatic, ring system to a conjugated porphyrinoid backbone. Incorporation of substructures, such as anthracene, at the *meso*-position,^[4c] and naphthyl^[4d] or azulene^[4b] to the porphyrin core have resulted in molecules with long-wavelength absorption up to 855 nm and large two-photon cross sections for near-infrared excitation.^[4b] The advanced optical properties of these motifs are realized in spite of the fact that none of these constructs are rigidly planar and fully conjugated across the entirety of the porphyrinoid backbone. Thus, development and understanding of unusual synthetic methodologies toward fusion of peripheral, aromatic substituents is important for further enhancement of the optical properties of these versatile porphyrinoid chromophores.

In a conceptually unrelated work, Smith et al.^[7] showed that alkynes fused to the β,β' -positions of one of the four

[a] Dr. L. J. K. Boerner, S. Mazumder, Dr. M. Pink, Prof. M.-H. Baik, Prof. J. M. Zaleski
Department of Chemistry and Molecular Structure Center
Indiana University, Bloomington, Indiana 47405 (USA)
E-mail: mbaik@indiana.edu
zaleski@indiana.edu

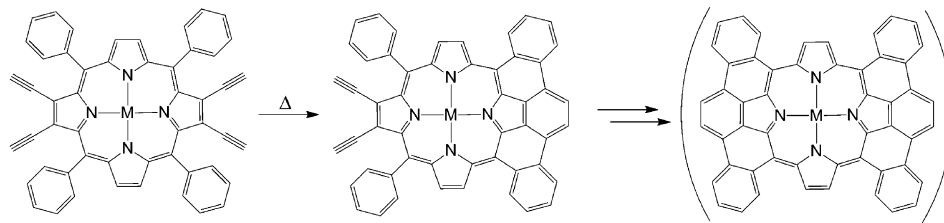
Supporting information for this article, including details about experimental methods, estimation of barrier heights for **4-TS** and **9-TS** as well as X-ray structure data collection, structure solution, and refinement for **Ni2b**, **Zn2c**, **H3a**, and **H8a**, including CIF files, is available on the WWW under <http://dx.doi.org/10.1002/chem>.

backbone pyrroles could be thermally activated at high temperatures (190 °C) to undergo Bergman cyclization, forming a six-membered, 1,4-phenyl diradical capable of addition to the adjacent phenyl rings at the macrocycle *meso*-positions.^[8] This thermal rearrangement affords three new C–C bonds per dialkyne, and upon rearomatization through H₂ elimination, extends the porphyrin conjugation, redshifting the π – π^* electronic transitions. The resulting piceno unit is a remarkable example of chemical stitching of adjacent aromatic segments that could find utility in chemical synthesis. Subsequent work on dialkynylporphyrins with hydrogen or halogen substitution at the termini positions^[9] demonstrated that the high thermal barrier to this process could be reduced by a steric or an inductive effect; this latter observation has been computationally purported to reduce electron repulsion in the transition state.^[10] The decreased barrier to the primary cyclization event also permits the photocyclization process to occur at 10 °C, further promoting formation of the extended, aromatized, piceno product under accessible conditions. Attachment of a 1,2-diamino arenediynes at the β,β' -pyrrole positions can also generate a cyclized product, albeit without creation of the extended piceno-unit.^[11]

The tools to extend this conceptual framework to penta-, hexa-, and octaalkynyl porphyrins to create larger aromatic constructs by a multistep, ring-closure event is established^[12] and several of these constructs have been crystallographically characterized.^[13] Interestingly, across this series, a redshift in the electronic spectrum of B and Q bands of 40 nm is observed, or about 13 nm per alkyne unit. As electronically attractive as this series is, formation of a single chemical product by Bergman cyclization/*meso*-phenyl-ring substitution is unfortunately hindered with addition of each successive dialkyne pair, to the limit at which no isolable aromatized structure is detected upon either heating or photochemical activation. This suggests that the reaction profile is either dominated by side-product (i.e., polymer) formation, or that a considerable energetic penalty exists to more than one cyclization event—likely caused by molecular strain communicated throughout the macrocycle backbone. This hypothesis is supported by the solid-state thermal cyclization temperatures of the octaalkynylporphyrins, which increase as the deviation of the macrocycle from planarity increases,^[13] suggesting that the strain of the molecule can override the thermodynamic gains of formation of a large extended π system, which should be the thermodynamically favored structure.

As a mean to determine which of these issues are responsible for the observed reaction profile and specifically define the origin and magnitude of molecular strain in these extended π structures, four alkyne units were installed at the antipodal β,β' -pyrrole positions. The resulting tetraalkynyl-

porphyrins have the potential to cyclize and systematically aromatize the two halves of the macrocycle backbone; this creates the highly conjugated bispicenoporphyryin skeleton (Scheme 1). If structural flexibility permits the formation of six additional C–C bonds, the bispicenoporphyryin product



Scheme 1. Bergman cyclization of tetraalkynylporphyrins.

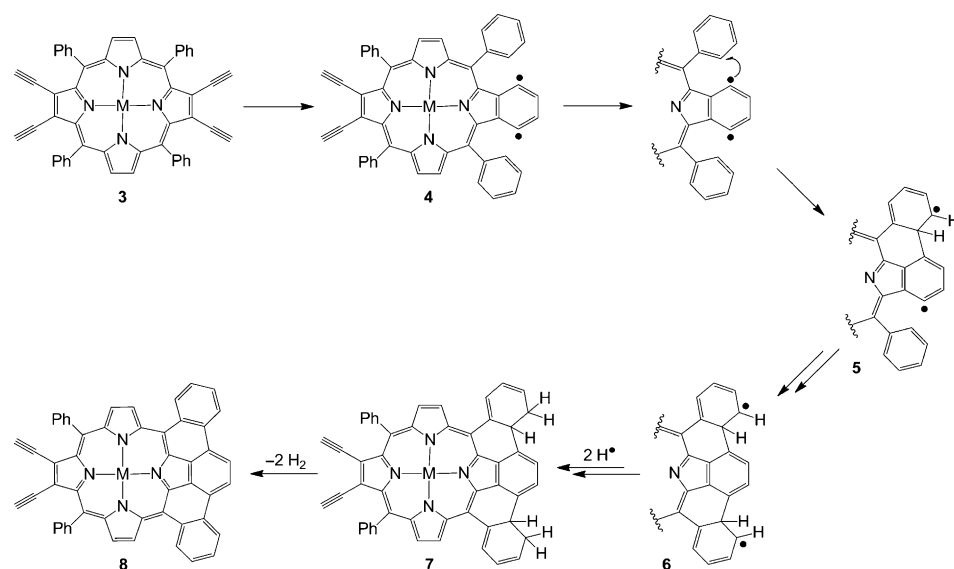
should be a highly aromatized, thermodynamically stable structure. Because polymerization always accompanies single-enediynes-unit cyclization steps,^[14] a precise assessment of reaction progress and mechanism is difficult. DFT calculations are therefore used to computationally probe the single and double cyclization/rearomatization events along the reaction profile to the bispicenoporphyryin product. As an additional probe of molecular strain, computational evaluation of the *meso*-phenyl-substituted base structure, together with hydrogen and ethenyl derivatives, was carried out to examine the contribution of steric crowding to the pyrrole-ring distortion across the structure, and the effect of this distortion on the electronic energy of the system and corresponding reaction barriers along the reaction profile were evaluated.

Results and Discussion

Syntheses: A series of new compounds were prepared by using 5,10,15,20-tetraphenylporphyrin (TPP) as a starting material.^[15] The synthesis involves selective bromination at the antipodal porphyrin positions by refluxing five equivalents of *N*-bromosuccinimide (NBS) with TPP in CHCl₃ for 24 h.^[16] Bromination occurs quite readily and affords 2,3,12,13-tetrabromo-5,10,15,20-tetraphenylporphyrin (**1a**) in high yield (80%).

Nickel is inserted into the macrocycle by refluxing **1a** in a solution of Ni(OAc)₂·4H₂O in acetic acid and chloroform, and the product is isolated as the red–purple crystalline (2,3,12,13-tetrabromo-5,10,15,20-tetraphenylporphyrinato)-nickel(II) (**1b**) in 89% yield (see Scheme 2). The brominated 2,3,12,13-positions were ethynylated by treating **1** with six equivalents of trimethyl(trimethylstannylethynyl)silane and a Pd⁰ catalyst in an inert atmosphere. Addition of the trimethylsilylethynyl units is a facile reaction and affords the 2,3,12,13-tetrakis(trimethylsilylethynyl)-5,10,15,20-tetraphenylporphyrins (**2a,b**) in high yields ($\geq 75\%$).

ability to isolate **8** from solution suggests that sequential cyclization of each half of the molecule is the plausible path of reaction. Within this theme, the proposed mechanism (Scheme 3), adapted from Smith et al.,^[7] involves thermal



Scheme 3. Proposed mechanism for the stepwise Bergman cyclization of tetraalkynylporphyrins.

activation of one dialkynyl unit to generate the bis(1,4-diradical) species **4**. The radicals are then transferred to the adjacent *meso*-phenyl rings by electrophilic aromatic substitution to afford species **6**, which is quenched by two successive hydrogen transfers from the H⁺ donor to give the tetrahydro species **7**. The reduced aromatic structure is then oxidized upon workup, which results in the monocyclized, porphyrinic enediyne **8**. Due to the radical nature of the reaction and abundance of reactive alkynes, polymeric and oligomeric products are readily observed from this type of reaction^[19] and serve as an obstacle to achieve high yields. Initial attempts to generate **13** saw a high degree of polymerization, discernible as a layer of a sticky black substance on the sides and bottom of the reaction flask. CHD concentrations were then iteratively varied to achieve a better ratio of hydrogen donor to reactant, and the qualitative amounts of polymerized material were minimized. However, the presence of the fully cyclized bispiceno[20,1,2,3,4,5,10,11,12,13,14,15-*fg hij*]porphyrin product (**13**) has only been detected in trace amounts by mass spectrometry. When toluene was substituted for chlorobenzene/benzene and CHD, which acts as both solvent and hydrogen donor, the amounts of side product were further diminished, but polymerization was still the dominant reaction pathway. It is unknown at which step in the mechanism the oligomerization/polymerization occurs, but diradical **6** is a likely candidate, because bimolecular radical coupling or addition is competitive with hydrogen abstraction by **6** to form **7**. In fact, both dimers and trimers of the porphyrin product have been detected by mass spectrometry. This leads to the question of whether the inability to isolate **13** is simply due to poor quenching of the

intermediates, or more likely, the result of higher reaction barriers associated with the second cyclization event.

Structures of tetraalkynylporphyrins: Compound **3a** crystallizes as brown blocks in a monoclinic space group by slow evaporation from a chlorobenzene/methanol cosolvent system. A variety of methods and solvents were employed to grow crystals of compounds **3b** and **3c**, but crystals obtained for both proved too small for structure determination. To establish geometric parameters for these molecules, DFT-computed structures for **3b–c** were obtained (Table 2). The crystal structure of **3a** was also compared to the computational counterpart to confidently demonstrate the ability of the quantum calculations to reliably reproduce/predict the structures of the metallated porphyrins (Figure 1).

Table 2. Structural parameters for tetraalkynylporphyrins **3a–c**.

	Alkyne termini ^[a] [Å]	CS _x ^[b] [Å]	CS _y ^[b] [Å]	C _α –N–C _α	C _α –C _{meso} –C _α	C _α –C _{meso} –C _{meso} [Å]	Alkyne SB ^[e] [Å]	Alkyne TB ^[f] [Å]
3a crystal	4.11	2.08	2.07	106.3 ^[c]	126.2 ^[d]	1.40	1.42	1.19
3a model	4.13	2.12	2.06	106.5 ^[c]	126.1 ^[d]	1.42	1.41	1.22
3b model	4.17	1.95	1.91	106.9 ^[c]	120.8 ^[d]	1.40	1.41	1.22
3c model	4.13	2.12	2.06	106.5 ^[c]	126.1 ^[d]	1.41	1.41	1.22

[a] Terminal C–C distance. [b] Core size or M–N distance; in 2H porphyrins, N–N distance was measured and divided by two. The *x* axis is defined as the horizontal axis, and *y* as the vertical axis. [c] Angle measured for alkyne-substituted pyrroles, in degrees. [d] Angle reported for *meso*-position adjacent to measured pyrrole ring, in degrees. [e] Single bond. [f] Triple bond.

The X-ray and calculated structures of **3a** are in excellent agreement; the C_β–alkyne single bond, C_α–C_{meso} distance, and core size in the *y* direction are all within 0.01 Å. Only very minor differences in the alkyne termini distance, triple-bond length, and core size in the *x* direction exist; this indicates a high degree of accuracy in the calculated structures. The nature of this agreement allows the use of calculated structures instead of X-ray crystal structures for **3b–c**. Notable parameters for these include core size, a significant structural parameter in discussing planarity of porphyrins,^[20] which is 0.2 Å smaller for **3b** than for **3a** or **c**. This feature is common for Ni^{II} porphyrins, and leads to distinctively ruf-

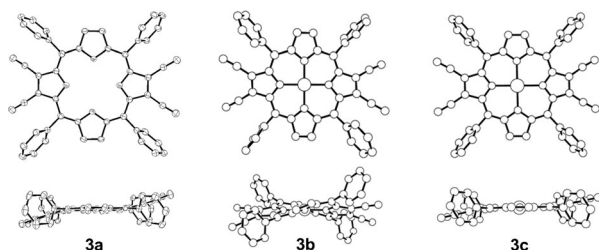


Figure 1. X-ray crystal structure of **3a** and computed structures for tetraalkynylporphyrins **3b–c**.

fled structures for substituted Ni^{II} porphyrin derivatives.^[5,20a,21]

The degree of the ruffling can be seen in the calculated deviation from a planar geometry for the tetraalkynylporphyrins, illustrated in Table 3 and Figure 3. Compound **3b** exhibits the classic ruffled conformation, showing a planar deviation of 0.322 Å. As a result, the alkynes also distort away from each other and cause a large alkyne termini distance (4.17 Å). For **3a** and **c**, the main porphyrin core is relatively flat, with deviations from the plane of 0.102 and 0.055 Å, respectively, from the idealized porphyrin framework. The Zn^{II} compound **3c** is slightly more planar than the free-base analogue, as is common for Zn^{II}TPP derivatives. The dialkyne units in both structures point slightly above and below the main porphyrin plane, ± 0.88 Å for the alkyne termini carbon atoms, due to the steric encumbrance of the *meso*-phenyl groups. However, the alkyne pairs lie planar to each other and have respective alkyne termini distances of 4.11 and 4.13 Å.

Partial thermal Bergman cyclization of **3a–c** produces new structures **8a–c** that are highly distorted (Figure 2) due to formation of three new C–C bonds: one from the devel-

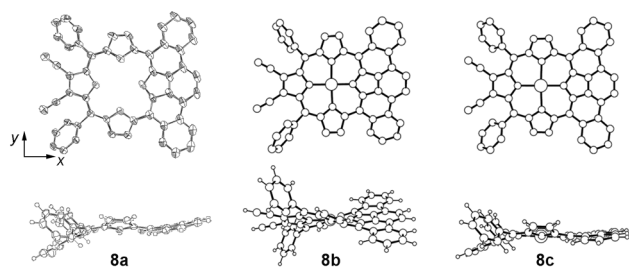


Figure 2. Structures of monocyclized porphyrinic enediynes.

oping benzyne ring, and two more from the radical addition at the 1,4-positions of the newly formed ring adjacent to the *meso*-phenyl substituents. The resulting aromatic system flattens and forces the rest of the molecule into a distorted geometry. For **8a** and **c**, this structural distortion subsequently increases the steric interaction on the opposite side of the molecule between the remaining dialkyne unit and the adjacent *meso*-phenyl rings. To minimize this unfavorable interaction, the entire porphyrin distorts to a pseudo-saddled conformation. Thus, as a result of the cyclization of

one side of the molecule, the remaining antipodal alkynes are displaced farther out of the plane of the porphyrin, and away from the remaining *meso*-phenyl rings; this in turn also forces the two remaining alkynes apart from each other. In **8a**, the alkyne termini distance increases from 4.11 to 4.27 Å, and from 4.13 to 4.23 Å for **8c**. Because the alkyne termini distance is a significant factor in the cyclization reactivity, this intuitively understandable increase of the alkyne distance provides one explanation for the inability to obtain fully cyclized structures from the reaction mixture. The cyclization of the first enediyne unit results in a nearly threefold increase in deviation from the plane of **8a** (0.102 to 0.288 Å), and a nearly fivefold increase in deviation from the plane of **8c** (0.055 to 0.269 Å; Figure 3, Table 3). In addi-

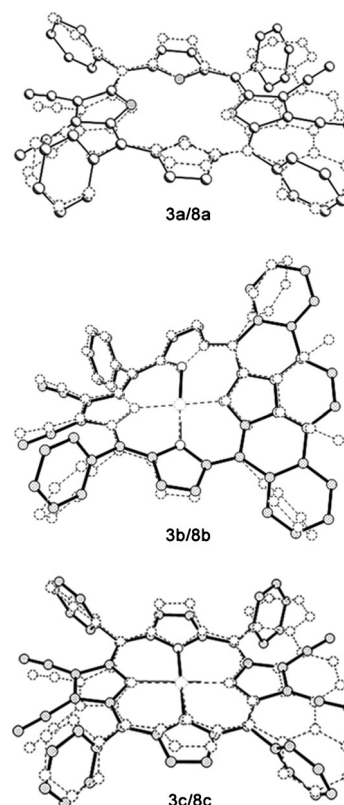


Figure 3. Structural overlays of deviation from plane for **3** (solid lines) and the subsequent cyclized structures **8** (dotted lines).

tion to these changes, the main core of the porphyrin undergoes significant transformations as well. The core of all compounds becomes antisymmetric upon cyclization (Table 2 and Table 4). For the free-base tetraalkyne **3a**, CS_x and CS_y are nearly equivalent at 2.08 and 2.07 Å, respectively. Upon cyclization, however, the core is forced to increase in size along the *y* direction ($CS_y = 2.17$ Å, in the direction along the length of the piceno unit) and compress along *x* ($CS_x = 1.95$ Å) to accommodate the expanded π -piceno unit. Whereas the flexible free-base porphyrin core can accommodate these structural changes, the more rigid Zn^{II} structure is less likely to do so. Similar to **3a**, the Zn^{II} porphyrin

Table 3. Calculated deviation from plane^[a] for porphyrinic enediynes **3** and **8** [Å].

	Mean ^[b]	NA _{pyrrole} ^[c]	NB _{pyrrole} ^[d]	C _{alkyne} ^[e]
3a crystal	0.102	-0.192	0.192	-0.886
8a crystal	0.288	-0.302	0.036	-1.584
3b model	0.322	0.034	0.056	-0.674
8b model	0.336	0.010	0.016	0.760
3c model	0.055	0.091	-0.091	0.080
8c model	0.269	0.279	0.014	-0.115

[a] Deviation of the indicated atom from the idealized planar structure. [b] The mean deviation of the 24 core atoms of the porphyrin macrocycle from the idealized planar structure. [c] Nitrogen of cyclized/enediyne pyrrole ring. [d] Nitrogen of uncyclized pyrrole ring. [e] Alkyne termini C for uncyclized enediyne.

Table 4. Structural parameters for porphyrinic enediynes **8**.

	Alkyne termini ^[a] [Å]	CS _x ^[b] [Å]	CS _y ^[b] [Å]	\angle C _α -N-C _α	\angle C _α -C _{meso} -C _α	C _α -C _{meso} [Å]	New C-C [Å]
8a crystal	4.27	1.95	2.17	104.8 ^[c]	120.3 ^[d]	1.39	1.44
8a model	4.19	1.97	2.17	105.0 ^[c]	120.7 ^[d]	1.41	1.46
8b model	4.13	1.89	1.95	106.2 ^[c]	116.1 ^[d]	1.39	1.41
8c model	4.23	2.03	2.11	107.5 ^[c]	120.5 ^[d]	1.41	1.41

[a] Terminal C-C distance. [b] M-N distance; in 2H porphyrins, N-N distance was measured, then divided by two. The *x* axis is defined as the horizontal axis and *y* as the vertical axis given in Figure 2. [c] The angle measured is the pyrrole on the new benzene ring in **8**, measured in degrees. [d] Angle measured was from *meso*-position adjacent to measured pyrrole ring, in degrees.

3c has a relatively symmetrical core size, with CS_x and CS_y distances of 2.12 and 2.06 Å, respectively. In cyclized **8c**, these distances shift to CS_x=2.03 and CS_y=2.11 Å; this highlights that the presence of Zn^{II} in the cavity restricts the divergence of the porphyrin from a symmetric core and leads to diminished change relative to the free-base analogue. Nonplanar Zn^{II} porphyrins are known, but they are exceedingly rare and are only observed when Zn^{II} has a coordinating axial ligand.^[22] Because only a very small amount (trace yield) of monocyclized Zn^{II} porphyrin can be isolated from solution, it appears that the half-cyclized Zn^{II} structure is highly susceptible to both further cyclization reactions, and competing side reactions that occur in the high-temperature solution. Distorted Zn^{II} porphyrins have been shown to be more susceptible to oxidation,^[22b] and strained, exocyclic Zn^{II} porphyrins in particular can react with ambient oxygen to form decomposition products.^[3c]

The compound **8b** displays fewer structural distortions upon cyclization than **8a** or **8c**. The deviation from the plane differs very little from the uncyclized tetraalkyne, that is, <0.02 Å. Unlike the free-base and Zn^{II} derivatives, the core size changes only very slightly; CS_x decreases from 1.95 to 1.89 Å, whereas CS_y increases from 1.91 to 1.95 Å. In addition, the alkyne-termini separation actually decreases slightly from 4.17 to 4.13 Å.

Electronic spectroscopy: Representative electronic absorption spectra for **3a** and **8a** are shown in Figure 4. The tetraalkynyl **3a** exhibits a B band at λ=441 nm, with a molar

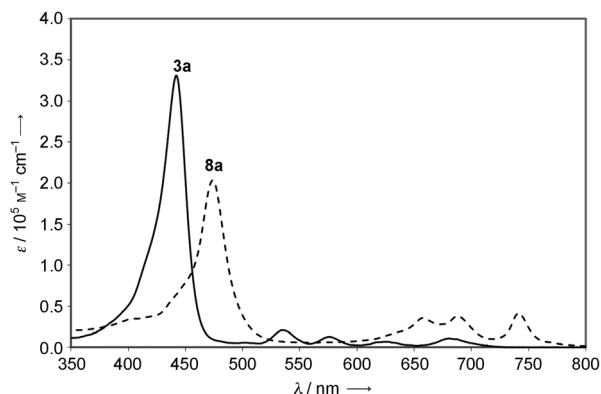


Figure 4. Absorption spectra for **3a** (solid line) and cyclized **8a** (dashed line).

absorptivity of $3.41 \times 10^5 \text{ M}^{-1} \text{ cm}^{-1}$. The four Q bands (535, 574, 627, and 686 nm) are a distinctive feature for free-base porphyrins, and indicate *D*_{2h} symmetry for the π-electron-conjugated ring system. The absorption spectrum for cyclized product **8a** is bathochromatically shifted due to the increased aromaticity, with the B band at λ=472 nm (ε = $1.95 \times 10^5 \text{ M}^{-1} \text{ cm}^{-1}$). The three discernable Q bands fall at 636, 658, 688, and 741 nm with extinction coefficients ranging from 1.84×10^5 to $4.13 \times 10^5 \text{ M}^{-1} \text{ cm}^{-1}$. It is known that structural perturbations, such as the addition of fused benzene rings, break the accidental degeneracy of the 1a_{1u} and 1a_{2u} HOMO set.^[23] This diminishes the ideally forbidden and allowed characters of the Q and B transitions, respectively, and causes the Q bands to gain intensity, at the expense of the B band.^[5h,23,24]

Computed reaction profiles: The mass-balanced^[25] reaction profile for Bergman cyclization of free-base tetraalkynylporphyrin **3a** can be seen in Figure 5 and Figure 6. As expected, the overall process is highly exothermic as a result of formation of π-extended porphyrin **13** in which six new C-C σ bonds have been formed in place of four π bonds in **3a**. Aromatization of two equivalents of CHD into benzene and release of four equivalents of H₂ molecules also favor the overall reaction equilibrium entropically. The fully cyclized and rearomatized product **13** lies 245.1 kcal mol⁻¹ below starting material **3**. The overall reaction profile has several steps and a total of six calculated reaction barriers. The first step affords the stable, intermediate, 1,4-diradical from the tetraalkynylporphyrin **3** by traversing the transition state **3-TS**, which has a barrier of 17.4 kcal mol⁻¹.^[26] The product of this reaction, diradical **4**, reacts stepwise with each adjacent *meso*-phenyl moiety, first to form the separated diradical **5**. This transient intermediate then adds to the second *meso*-phenyl ring to form diradical **6**. The addition of two equivalents of H[•] is expected to be a fast reaction, thus we assume

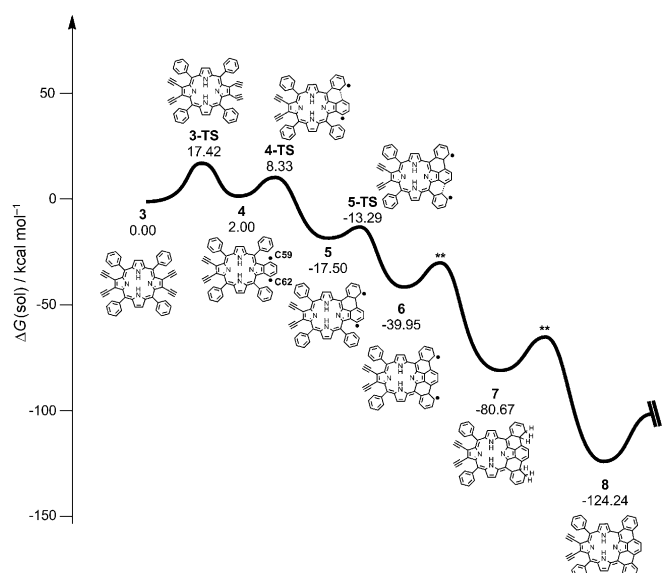


Figure 5. Reaction profile for the first cyclization of the Bergman cyclization of tetraalkynylporphyrin.

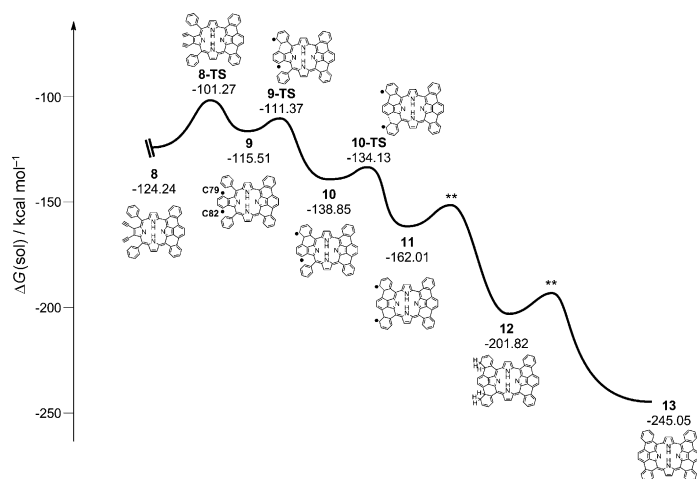


Figure 6. Reaction profile for the second cyclization of the Bergman cyclization of tetraalkynylporphyrin.

that both equivalents add simultaneously to give the quenched species **7**, which lies $80.7 \text{ kcal mol}^{-1}$ below the starting enediyne. The transition state between **6** and **7** cannot be calculated easily, due to difficulty to calculate the proper reaction trajectory for this intermolecular reaction, but we expect it to be relatively low in energy. Likewise, the release of two molecules of H_2 to form the rearomatized, half-cyclized **8** is also expected to be associated with a low barrier, which cannot be modeled reliably.^[27]

The cyclization mechanism of the second enediyne, shown in Figure 6, is analogous to the first half: Compound **8** traverses **8-TS** with a barrier height of $23.0 \text{ kcal mol}^{-1}$ to form diradical species **9**, which is $8.7 \text{ kcal mol}^{-1}$ higher in energy than **8**. Subsequently, one radical adds to the adjacent phenyl ring to form **10**, and the second adds to afford the

diradical intermediate **11**. Two equivalents of H^\cdot add to this species to give the quenched intermediate **12**, which eliminates two H_2 molecules to finally form the fully cyclized **13**, which lies $120.8 \text{ kcal mol}^{-1}$ below the half-cyclized **8** and an overall of $245.1 \text{ kcal mol}^{-1}$ below the starting porphyrinic enediyne **3**.

The diradical species **4–6** and **9–11** have been computed as open-shell singlets within a broken symmetry MO framework, to properly model the 1,4-diradicals resulting from Bergman cyclization as diradicals with the unpaired electrons adopting opposite spins.^[10a,12c,18a,28] Addition of *meso*-phenyl rings to these diradicals is facile with activation barriers of approximately 3 kcal mol^{-1} (see the Supporting Information for details). Spin densities from Mulliken population analysis are enumerated in Table 5 and show conver-

Table 5. Energies, C–C distance, and spin density for diradicals and associated transition states.

	$\Delta E(\text{gas})$ [kcal mol^{-1}]	$\Delta G(\text{sol})$ [kcal mol^{-1}]	C–C distance [\AA] ^[a]	Spin density ^[b]
3-TS	17.34	17.42	2.13	C59 0.01 C62 -0.01
4	-1.50	2.00	1.45	C59 0.75 C62 -0.75
8-TS	22.00	22.97	2.16	C79 0.00 C82 0.00
9	4.24	8.73	1.45	C79 0.79 C82 -0.78

[a] Length of new or forming C–C bonds. [b] Atomic spin densities from Mulliken analysis, as portion of an electron at 1,4-carbon atoms. Specific carbon atom positions are defined in Figure 5 and 6.

gence to the open-shell singlet states for species **4** and **9**. For diradical **4**, spin density at C59 and C62 (for numbering, see Figure 5) is approximately ± 0.75 , which shows strong diradical character at the 1,4-carbon atoms, and the radical orbital clearly shows unpaired alpha spin density on C59, and unpaired beta spin on C62 (Figure 7). Diradical **9** shows a marginally higher spin density of ± 0.79 at C79 and C82 (for numbering, see Figure 6). The two diradicals also differ in relative energies with **9** being $6.7 \text{ kcal mol}^{-1}$ higher in energy than **4** relative to the respective starting enediynes. The C–C distances for the new delocalized bonds are both 1.45 \AA , which is usual for a resonance-stabilized C–C double bond.

The transition states for the diradical formation (Table 5) show no significant diradical character; this is consistent with previous studies.^[18a,29] Structurally, the transition state is late, with C–C distances at 2.13 to 2.16 \AA . The alkyne triple bonds are slightly elongated, from 1.22 \AA in **3** and **8** to $1.26\text{--}1.27 \text{ \AA}$ in **3-TS** and **8-TS**, respectively; this shows that the bonds still retain significant triple bond character. Thus, the transition state can be characterized as structurally late, but electronically early. The most notable characteristic of **3-TS** and **8-TS**, however, is the difference in relative energy: **8-TS** lies $5.5 \text{ kcal mol}^{-1}$ higher than **3-TS**. Inspection of the differences in energy terms, summarized in Table 5, reveals that practically the same energy difference can be found in

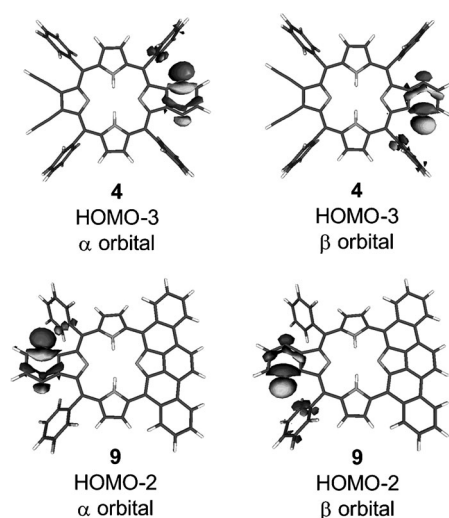


Figure 7. Isosurface plots (0.05 a.u.) of the MOs for **4** and **9** that show di-radical character.

the electronic component. A more detailed analysis suggests that the structural difference of how the enediynes are oriented in relation to the rest of the porphyrin system during the first and second cyclization is responsible for the energetic difference. As discussed above, **3** displays a planar porphyrin core, with the alkyne pairs pointing slightly above and below the plane, as shown in Figure 1. The *meso*-phenyl rings, which in **3** are almost orthogonal to the porphyrin π system, need to rotate into the plane to couple with the 1,4-diradical and to form the new C–C bonds. To accommodate this new piceno unit, the porphyrin core must elongate in the *y* direction; this in turn distorts the angles at the *meso* carbon atoms, and pushes the adjacent pyrrole moieties out of the plane. The overall effect is a loss of porphyrin planarity, which destabilizes the π system. This translates into a higher barrier for the second cyclization than the first and increases the likelihood that **8** will follow alternative, unproductive reaction pathways, such as polymerization, radical-radical coupling, or Stork acylation.^[30]

To probe how this strain impacts the transition states, two other porphyrinic enediyne models were considered, each with a smaller functional group at the porphyrin *meso*-position. Compound **19** has hydrogen at this position, and **14** ethenyl units (C₂H₃). Both systems are completely planar (Figure 8). The C–C distances and the diradical character in the respective transition states closely resemble those of the Ph system (Table 6). Activation barriers for the formation of 1,4-diradicals of these model systems were found to be similar for the first and second cyclization event. For C₂H₃, the activation energies are 20.0 and 19.8 kcal mol⁻¹, for first and second cyclization events, respectively, whereas they are 26.2 and 26.0 kcal mol⁻¹ for H (Table 6). These model systems differ from the phenyl (Ph)-substituted system in that for C₂H₃ the first cyclization requires 2.6 kcal mol⁻¹ higher activation energy, whereas the second cyclization is lower in energy by 3.2 kcal mol⁻¹ compared with the Ph-substituted

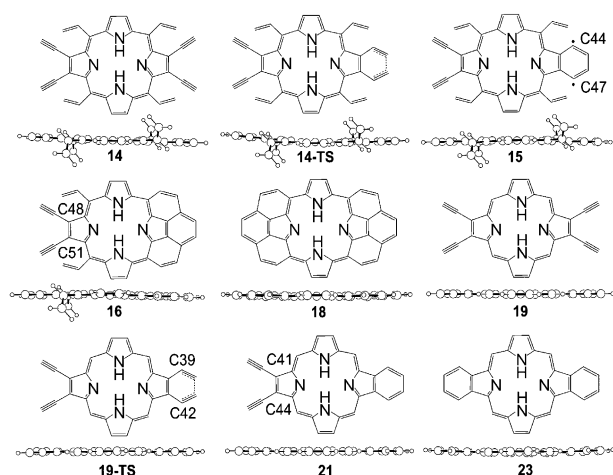


Figure 8. Structures of model-porphyrinic-enediyne systems with C₂H₃ and H at the *meso*-positions.

Table 6. Energies, C–C distance, and spin density for diradicals and associated transition states for model systems.

	$\Delta E(\text{gas})$ [kcal mol ⁻¹]	$\Delta G(\text{sol})$ [kcal mol ⁻¹]	C–C distances [Å] ^[a]	Spin density ^[b]
14-TS	19.35	19.97	2.16	C44 0.00
				C47 0.00
15	1.22	5.29	1.45	C44 0.81
				C47 -0.81
16-TS	19.02	19.79	2.17	C48 0.00
				C51 0.00
17	1.41	5.43	1.45	C48 -0.81
				C51 0.81
19-TS	25.25	26.19	2.10	C39 0.00
				C42 0.00
20	7.82	12.10	1.45	C39 -0.83
				C42 0.83
21-TS	25.09	26.00	2.15	C41 0.00
				C44 0.00
22	8.07	12.38	1.45	C41 -0.83
				C44 0.83

[a] Length of new or formed C–C bond. [b] Atomic spin densities from Mulliken analysis, as portion of an electron at 1,4-carbon atoms. Specific carbon atom positions are defined in Figure 8.

system. For H, both the first and second cyclizations are higher by 8.8 and 3.0 kcal mol⁻¹, respectively, compared to the Ph-substituted analogue. These model systems suggest that stabilization from an additional conjugated π system at the *meso*-position aids in making the cyclization feasible. The H-substituted derivative lacks this feature, resulting in a higher barrier of about 26 kcal mol⁻¹. Whereas this factor favors the first cyclization event for Ph relative to C₂H₃, the bulkiness of the *meso*-phenyl group perturbs the planarity of the porphyrin core in the second cyclization event; this makes it energetically more costly than C₂H₃.

Diradical character as assessed by Mulliken spin density (MSD) is reported in Table 6 for these model systems. For C₂H₃, diradicals of **15** and **17** both have MSDs of ± 0.81 , compared to the H system, in which diradicals **20** and **22** have spins of ± 0.83 . These values emphasize further that

the model systems reliably mimic the electronics of the real systems.

With the insight from the small model system at hand, we attempted to reproduce the electronic impact of the structural distortion, discussed above, in another computational experiment. An artificial 30° cant is introduced in the pyrrole rings relative to the plane of the porphyrin in **16** and this angle is fixed when the transition state of the second Bergman cyclization is calculated. Optimized geometries of **16** and **16'** are shown in Figure 9. Interestingly, the second

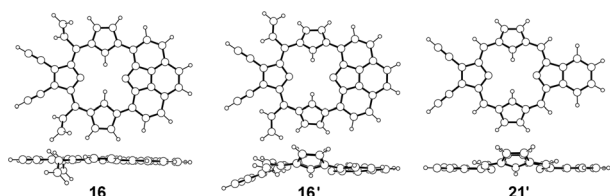


Figure 9. Comparison of optimized geometries of **16**, **16'** and **21'**. In **16'** and **21'** pyrroles are fixed at 30° cant.

cyclization barrier increases from 19.8 to 21.8 kcal mol⁻¹, as illustrated in Figure 10. Inspection of **16'** clearly shows significant bending of the enediyne moiety from the porphyrin plane as a result of canting of the pyrrole. This is reflected in an activation-barrier increase by 2.0 kcal mol⁻¹ from **16** to **16'**. This distortion perturbs the resonance gained from the conjugation of the *meso*-position into the porphyrin system, and raises the barrier for the second cyclization. However, for H, similar canting of pyrrole rings showed no change in the activation barrier (**21-TS** and **21'-TS** in Figure 10). Thus the distortion that the first cyclization event causes to the porphyrin ring in the Ph-substituted system is the cause of the increased barrier to the second cyclization event, due to the decreased stabilization from reduced π overlap.

Conclusion

Heating of a new series of free-base, Ni^{II}, and Zn^{II} 2,3,12,13-tetra(ethynyl)-5,10,15,20-tetraphenyl porphyrins promotes two of the four ethynyl moieties to undergo Bergman cyclization to afford the monocyclized 2,3-diethynyl-5,20-diphenylpiceno[10,11,12,13,14,15-*ijklmn*]porphyrin in 30%, 10%, and trace yields, respectively. No fully cyclized bis(piceno[20,1,2,3,4,5,10,11,12,13,14,15-*fg hij*])porphyrin was isolated from the reaction mixture. The X-ray and computational structures of picenoporphyrin products show significant deviation from the idealized planar structure as well as from that of the starting material. Thus the distortion on the porphyrin backbone imparted by the newly formed piceno unit is clearly a complicating factor in the second cyclization event. Computation of the reaction coordinates with DFT at the PWPW91/cc-pVTZ(-f) level coupled to a continuum solvation model reveal that the barrier to cyclization of the second pair of ethynyl groups was found to be 5.5 kcal mol⁻¹

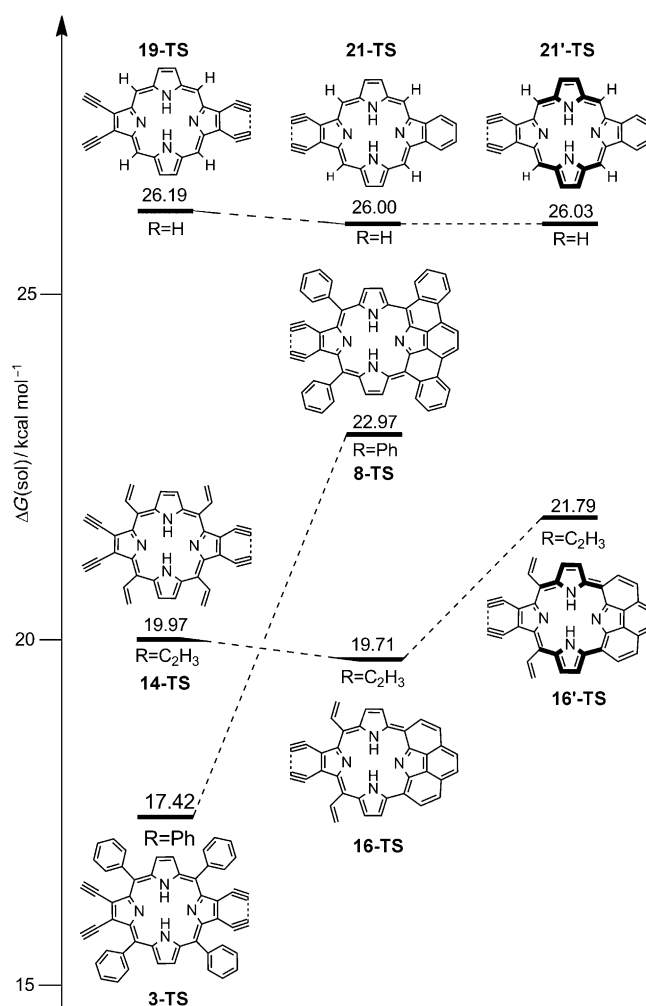


Figure 10. Diagram that illustrates the relative energy changes of the cyclization transition states upon substitution at the *meso*-position in porphyrinic enediynes. Bonds in bold indicate molecules frozen in the distorted geometry (pyrroles are fixed at 30° cant).

higher than to the first; this suggests a negative cooperative effect and a significantly slower rate for the second cyclization. Cyclization reactions for model porphyrinenediynes with ethene and H functionality at the *meso*-positions were also found to have the same barrier to diradical formation for the second cyclization event as for the first in these highly planar molecules. Enforcing an artificial 30° cant in two of the pyrrole rings of the porphyrin increases the second barrier by 2 kcal mol⁻¹ in the ethene model, indicating that disruption of the π conjugation in the extended porphyrin structure is the cause of the increased barrier to the second cyclization event. Combined, this suggests that maintaining a planar aromatic structure is paramount to promote combined or tandem cyclization reactions in the pursuit of extended π structures.

Experimental Section

Materials and general procedures: All chemicals and solvents used were of the highest purity available from Aldrich and Strem. Air-sensitive reactions were carried out under nitrogen by using Schlenk techniques and air-sensitive compounds were handled in an inert-atmosphere dry box. Compounds were purified by flash chromatography with activated neutral aluminum oxide or silica gel. All NMR (^1H and ^{13}C) spectra were recorded on a VXR 400, i400, or Gem 300 NMR spectrometer with the residual proton resonance of the solvent as an internal reference. Infrared spectra (KBr) were measured with a Nicolet 510P FTIR spectrophotometer. MALDI-TOF data were obtained with a Bruker Biflex III MALDI-TOF mass spectrometer. ESI and EI-HRMS spectra were recorded on PE-Sciex API III Triple Quadrupole and Thermo Finnigan MAT 95 XP high-mass-resolution spectrometer, respectively. Elemental analyses were obtained from Robertson Microлит Laboratories. Electronic absorption spectra were acquired on a Perkin-Elmer Lambda 19 UV/Vis/near-IR spectrometer. All DSC traces were measured on a TA Instruments Q10 DSC at a heating rate of $10^\circ\text{C min}^{-1}$.

Porphyrin precursors syntheses: 5,10,15,20-Tetraphenylporphyrin was synthesized by using the Adler method (yield: 20%).^[15] $^1\text{H NMR}$ (CDCl_3): $\delta=7.76\text{--}7.80$ (m, 12H, *meso*-ArH), 8.25 (dd, $J=1.6$, 1.6 Hz, 8H, *meso*-ArH), 8.88 ppm (s, 8H, β -pyrrolic H).

Compound 1a: Compound **1a** was prepared as described by Crossley (yield: 80%).^[16] $^1\text{H NMR}$ (CDCl_3): $\delta=7.76\text{--}7.81$ (m, 12H, *meso*-ArH), 8.18 (dd, $J=1.5$, 2.1 Hz, 8H, *meso*-ArH), 8.70 ppm (s, 4H, β -pyrrolic H).

Compound 1b: To a solution of **1a** (1.0 g, 1.1 mmol) in CHCl_3 (500 mL), a solution of $\text{Ni}(\text{OAc})_2\cdot 4\text{H}_2\text{O}$ (0.60 g, 2.4 mmol) in acetic acid (20 mL) was added. The reaction mixture was stirred at reflux temperature for 8 h. After completion of the reaction, the reaction mixture was cooled to room temperature and washed with water (4×500 mL). The organic layer was dried over Na_2SO_4 and concentrated under reduced pressure. The crude product was triturated with MeOH and filtered to afford red-purple crystals (yield: 89%). $^1\text{H NMR}$ (CDCl_3): $\delta=7.72\text{--}7.62$ (m, 12H, *meso*-ArH), 7.90–7.84 (m, 8H, *meso*-ArH), 8.54 ppm (s, 4H, β -pyrrolic H); MALDI-TOF-MS m/z : 986 [M] $^+$.

Compound 2a: To $(\text{Ph}_3\text{P})_2\text{Pd}$, a solution of **1a** (500 mg, 0.538 mmol) in dry THF (30 mL) was added at room temperature. Trimethyl(trimethylstannylethynyl)silane (842 mg, 3.23 mmol) in dry THF (15 mL) was then added to the reaction mixture and heated to reflux ($70\text{--}80^\circ\text{C}$) for 6 h. The solvent was removed under reduced pressure and the resulting solid was purified by activated, neutral, aluminum-oxide, column chromatography with 40% CH_2Cl_2 in hexane (yield: 90%). $^1\text{H NMR}$ (CDCl_3): $\delta=0.18$ (m, 36H, $4(\text{CH}_3)_3\text{Si}$), 7.69–7.73 (m, 8H, *meso*-ArH), 7.78–7.81 (m, 4H, *meso*-ArH), 8.17 (d, $J=7.2$ Hz, 8H, *meso*-ArH), 8.63 ppm (s, 4H, β -pyrrolic H); $^{13}\text{C NMR}$ (CDCl_3): $\delta=1.01$, 99.35, 109.67, 120.55, 127.40, 128.88, 129.42, 134.23, 135.76, 140.49, 141.60, 151.75 ppm; IR (KBr): $\tilde{\nu}=629$, 657, 702, 757, 800, 853, 898, 1001, 1031, 1100, 1140, 1243, 1470, 1599, 2131, 2926, 3365 cm^{-1} ; HRMS (EI): m/z : calcd for $\text{C}_{64}\text{H}_{62}\text{N}_4\text{Si}_4$: 999.4124; found: 999.4152.

Compound 2b: To a suspension of **1b** (0.95 g, 0.96 mmol) and $(\text{Ph}_3\text{P})_2\text{Pd}$ (0.15 g, 0.13 mmol) in dry THF (80 mL), a solution of trimethyl(trimethylsilylethynyl)titanium (1.6 g, 6.10 mmol) in dry THF (40 mL) was added. The reaction mixture was stirred at $70\text{--}75^\circ\text{C}$ for 6 h. After completion of the reaction, the mixture was cooled to 25°C and the solvent was evaporated under reduced pressure. The crude solid was purified on activated, neutral, aluminum-oxide column by using 15% CH_2Cl_2 in hexane as eluent (yield: 87%). Crystals for X-ray diffraction were obtained by slow diffusion from dichloromethane/hexanes. $^1\text{H NMR}$ (CDCl_3): $\delta=0.14$ (s, 36H, $4(\text{CH}_3)_3\text{Si}$), 7.59 (dd, $J=8.0$, 6.8 Hz, 8H, *meso*-ArH), 7.68 (dd, $J=7.6$, 7.2 Hz, 4H, *meso*-ArH), 7.89 (d, $J=7.2$ Hz, 8H, *meso*-ArH), 8.44 ppm (s, 4H, β -pyrrolic H); $^{13}\text{C NMR}$ (CDCl_3): $\delta=1.03$, 98.57, 110.34, 119.53, 127.39, 132.59, 133.348, 134.53, 140.09, 140.79, 145.27 ppm; IR: $\tilde{\nu}=631$, 644, 662, 697, 720, 745, 757, 792, 833, 894, 995, 1005, 1020, 1073, 1131, 1156, 1176, 1200, 1247, 1338, 1372, 1442, 1493, 1520, 1599, 2139, 2954 cm^{-1} ; UV/Vis (CH_2Cl_2): λ_{max} (ϵ) = 447.0 (35.35), 512.0 (0.83), 551.5

(1.70), 615.0 nm ($3.50\times 10^{-4}\text{ M}^{-1}\text{ cm}^{-1}$); MALDI-TOF-MS: m/z : 1054 [M] $^+$; HRMS (EI): m/z : calcd for $\text{C}_{64}\text{H}_{60}\text{N}_4\text{NiSi}_4$: 1055.2234; found: 1055.3373.

Compound 2c: To a solution of **2a** (500 mg, 0.501 mmol) in CHCl_3 (200 mL), 1.2 equivalents of $\text{Zn}(\text{OAc})_2\cdot \text{H}_2\text{O}$ (130 mg, 0.601 mmol) in MeOH (50 mL) were added. The reaction mixture was stirred at room temperature for 1 h to afford a green solution. The solvent was removed under reduced pressure and the resulting solid was purified by silica-gel column chromatography with CH_2Cl_2 /hexane (1:1) (yield: 95%). Crystals for X-ray diffraction were obtained by slow diffusion from dichloromethane/methanol. $^1\text{H NMR}$ (CDCl_3): $\delta=0.23$ (s, 36H, $4(\text{CH}_3)_3\text{Si}$), 7.63–7.68 (m, 8H, *meso*-ArH), 7.75–7.77 (m, 4H, *meso*-ArH), 8.06 (d, $J=7.2$ Hz, 8H, *meso*-ArH), 8.59 ppm (s, 4H, β -pyrrolic H); $^{13}\text{C NMR}$ (CDCl_3): $\delta=-1.37$, 99.49, 110.65, 121.60, 127.14, 128.90, 133.16, 133.55, 134.94, 142.50, 147.34, 152.30 ppm; IR (KBr): $\tilde{\nu}=630$, 659, 698, 759, 795, 866, 895, 1002, 1024, 1072, 1121, 1173, 1245, 1321, 1352, 1485, 1598, 2136, 2955 , 3052 cm^{-1} ; HRMS (ESI): m/z : calcd for $\text{C}_{64}\text{H}_{60}\text{N}_4\text{Si}_4\text{Zn}$: 1061.3181; found 1061.3212.

Compound 3a: To a solution of **2a** (200 mg, 0.200 mmol) in THF (40 mL), 1 M solution of TBAF in THF (1 mL) was added. The reaction mixture was stirred at room temperature for 2 h. After completion of the reaction, the solvent was evaporated and the resulting residue was dissolved in CH_2Cl_2 . This solution was washed with water, dried over Na_2SO_4 and evaporated under reduced pressure. The crude compound was purified by activated, neutral, aluminum-oxide, column chromatography with CH_2Cl_2 /hexane (1:1) as solvent (yield: 90%). Crystals for X-ray diffraction were obtained by slow diffusion from chlorobenzene/methanol. $^1\text{H NMR}$ (CDCl_3): $\delta=3.57$ (s, 4H, alkynyl H), 7.65–7.70 (m, 8H, *meso*-ArH), 7.78–7.83 (m, 4H, *meso*-ArH), 8.08 (d, $J=8.1$ Hz, 8H, *meso*-ArH), 8.83 ppm (s, 4H, β -pyrrolic H); $^{13}\text{C NMR}$ (CDCl_3): $\delta=90.58$, 120.47, 124.10, 128.62, 129.52, 134.19, 134.67, 140.04, 141.61 ppm; IR (KBr): $\tilde{\nu}=608$, 687, 699, 735, 768, 753, 801, 960, 1002, 1031, 1074, 1089, 1157, 1137, 1175, 1251, 1281, 1342, 1376, 1442, 1476, 1507, 1551, 1598, 1713, 1828, 1892, 2105, 3047, 3290 cm^{-1} ; UV/Vis (CH_2Cl_2): λ_{max} (ϵ) = 442.0 (34.14), 535.5 (2.19), 574.0 (1.41), 627.0 (0.76), 686.0 nm ($1.11\times 10^{-4}\text{ M}^{-1}\text{ cm}^{-1}$); elemental analysis calcd (%) for $\text{C}_{52}\text{H}_{50}\text{N}_4\cdot \text{H}_2\text{O}$: C 85.68, H 4.43, N 7.69; found: C 85.44, H 4.14, N 7.25.

Compound 3b: To a solution of **2b** (0.80 g, 0.76 mmol) in THF (150 mL), MeOH (75 mL) was added followed by the addition of water (7.5 mL) and K_2CO_3 (1.3 g, 9.40 mmol). The reaction mixture was stirred at 25°C for 24 h. After completion of the reaction, the solvent was evaporated to dryness. The purple solid was washed with water and purified on activated, neutral, aluminum-oxide, column by using CH_2Cl_2 /hexane (1:4) as eluent (yield: 80%). $^1\text{H NMR}$ (CDCl_3): $\delta=3.49$ (s, 4H, alkynyl H), 7.57 (dd, $J=7.6$, 7.2 Hz, 8H, *meso*-ArH), 7.68 (dd, $J=7.6$, 7.2 Hz, 4H, *meso*-ArH), 7.84 (d, $J=7.2$ Hz, 8H, *meso*-ArH), 8.70 ppm (s, 4H, β -pyrrolic H); $^{13}\text{C NMR}$ (CDCl_3): $\delta=90.49$, 119.10, 127.06, 128.52, 131.87, 133.43, 133.71, 139.78, 140.04, 144.08 ppm; IR (KBr): $\tilde{\nu}=633$, 697, 742, 793, 833, 889, 1022, 1071, 1116, 1198, 1340, 1442, 1514, 1599, 1807, 2096, 3047, 3289 cm^{-1} ; UV/Vis (CH_2Cl_2): λ_{max} (ϵ) = 440.0 (41.46), 557.0 (1.87), 609.0 nm ($3.64\times 10^{-4}\text{ M}^{-1}\text{ cm}^{-1}$); MALDI-TOF-MS: m/z : 766 [M] $^+$; elemental analysis calcd (%) for $\text{C}_{52}\text{H}_{28}\text{N}_4\cdot \text{H}_2\text{O}$: C 79.31, H 4.10, N 7.11; found: C 79.47, H 3.79, N 7.01.

Compound 3c: To a solution of **2c** (500 mg, 0.50 mmol) in THF (150 mL), 1 M solution of TBAF in THF (1 mL) was added. The reaction mixture was stirred at room temperature for 2 h. After completion of the reaction, the solvent was evaporated and the resulting residue was dissolved in CH_2Cl_2 . This solution was washed with water, dried over Na_2SO_4 , filtered, and evaporated under reduced pressure. The crude compound was purified by silica-gel column chromatography (yield: 55%). $^1\text{H NMR}$ (CDCl_3): $\delta=3.61$ (s, 4H, alkynyl H), 7.61–7.67 (m, 8H, *meso*-ArH), 7.76–7.78 (m, 4H, *meso*-ArH), 8.03 (d, $J=6.9$ Hz, 8H, *meso*-ArH), 8.82 ppm (s, 4H, β -pyrrolic H); $^{13}\text{C NMR}$ (CDCl_3): $\delta=90.61$, 121.26, 126.61, 128.22, 131.97, 133.22, 133.96, 142.13, 147.26, 151.71 ppm; IR (KBr): $\tilde{\nu}=619$, 673, 699, 746, 757, 766, 794, 831, 845, 891, 912, 976, 1009, 1033, 1072, 1105, 1166, 1177, 1194, 1245, 1321, 1345, 1441, 1490, 1575, 1598, 1702, 1817, 2091, 2919, 3305 cm^{-1} ; UV/Vis (CH_2Cl_2): λ_{max} (ϵ) = 442.0 (53.09), 571.0 (1.65), 617.5 nm ($3.47\times 10^{-4}\text{ M}^{-1}\text{ cm}^{-1}$); HRMS (ESI): m/z : calcd for $\text{C}_{52}\text{H}_{28}\text{N}_4\text{Zn}$ [$M+\text{H}$] $^+$ 773.1678; found: 773.1703.

Thermal cyclization of 3a: A solution of **3a** (20 mg, 0.028 mmol) in toluene (15 mL) was heated in a pressure tube at 115 °C for 2 h. The solvent was evaporated under reduced pressure and the resulting solid was purified by activated, neutral, aluminum-oxide, column chromatography by using 2% ethyl acetate in CH_2Cl_2 to produce **8a** and **13a** in 30% and trace yields, respectively. Characterization data for **13a**: MALDI-TOF MS: m/z : 707 $[\text{MH}]^+$. Characterization data for **8a**: Crystals for X-ray diffraction were obtained by slow diffusion from dichloromethane/methanol. $^1\text{H NMR}$ (CDCl_3): δ =3.62 (s, 2H, alkynyl H), 7.75 (dd, 2H, piceno-H), 7.75 (m, 6H, *meso*-ArH), 7.78 (q, 4H, *meso*-ArH), 8.16 (d, J =7.2 Hz, 4H, piceno-H), 8.49 (s, 2H, piceno-H), 8.59 (d, J =7.6 Hz, 2H, piceno-H), 8.74 (d, J =6.4 Hz 2H, piceno-H), 9.36 ppm (m, 4H, β -pyrrolic H); IR (KBr): $\tilde{\nu}$ =664, 698, 754, 795, 822, 850, 866, 965, 1001, 1081, 1442, 1552, 1710 cm^{-1} ; UV/Vis (CH_2Cl_2): λ_{max} (ϵ)=473.5 (20.33), 658.0 (3.56), 688.0 (3.78), 741.5 nm ($4.14 \times 10^{-4} \text{M}^{-1} \text{cm}^{-1}$); MALDI-TOF MS: m/z : 708 $[\text{M}]^+$; HRMS (internally calibrated MALDI-TOF-MS): calcd for $\text{C}_{52}\text{H}_{28}\text{N}_4$ $[\text{M}]^+$: 708.2314; found: 708.2416.

Thermal cyclization 3b: To a solution of **3b** (35 mg, 0.046 mmol) in chlorobenzene (15 mL), CHD (1.5 mL) was added. The mixture was stirred at 105 °C in a pressure tube for 1.5 h. The reaction mixture was cooled to room temperature, loaded on a silica-gel column, and eluted with hexane (500 mL) to remove the chlorobenzene. The column was further eluted with 50% CH_2Cl_2 in hexane to afford **8b** in 10% yield. $^1\text{H NMR}$ (CDCl_3): δ =3.47 (s, 2H, alkynyl H), 7.47 (dd, J =7.6, 7.2 Hz, 2H, piceno-H), 7.63 (dd, J =8.0, 7.2 Hz 4H, *meso*-ArH), 7.75–7.69 (m, 4H, *meso*-ArH), 7.89 (d, J =6.8 Hz 4H, piceno-H), 8.45 (s, 2H, piceno-H), 8.50 (d, J =8.0 Hz, 2H, piceno-H), 8.79 (d, J =4.8 Hz, 2H, β -pyrrolic H), 9.03 (d, J =8.0 Hz, 2H, piceno-H), 9.32 ppm (d, J =4.8 Hz, 2H, β -pyrrolic H); $^{13}\text{C NMR}$ (CDCl_3): δ =88.63, 96.12, 106.92, 121.31, 123.12, 124.24, 125.08, 125.63, 126.93, 128.36, 129.23, 129.42, 129.85, 132.70, 133.38, 136.60, 138.52, 138.60, 140.04, 145.47 ppm; IR (KBr): $\tilde{\nu}$ =574, 627, 662, 698, 762, 790, 820, 840, 879, 985, 1000, 1018, 1077, 1135, 1249, 1295, 1378, 1434, 1505, 2110, 3306 cm^{-1} ; UV/Vis (CH_2Cl_2): λ_{max} (ϵ)=472.0 (8.08), 587.0 (0.44), 635.0 nm ($7.76 \times 10^{-4} \text{M}^{-1} \text{cm}^{-1}$); MALDI-TOF-MS: m/z : 765 $[\text{M}+\text{H}]^+$, 764 $[\text{M}]^+$; HRMS (internally calibrated MALDI-TOF-MS): calcd for $\text{C}_{52}\text{H}_{26}\text{N}_4\text{Ni}$ $[\text{M}]^+$: 764.1511; found: 764.1479.

Thermal cyclization of 3c: A solution of **3c** (20 mg, 0.046 mmol) in toluene (15 mL) was stirred at 110 °C in a pressure tube for 2 h. Upon completion of the reaction, the solvent was removed under reduced pressure. The crude compound was purified by silica-gel column chromatography to afford **8c** in trace yields. MALDI-TOF-MS: m/z : 773 $[\text{M}+\text{H}]^+$.

CCDC-825981 (**H8a**), 825982 (**Zn2c**), 825983 (**H3a**), and 825984 (**Ni2b**) contain the supplementary crystallographic data for this paper. These data can be obtained free of charge from The Cambridge Crystallographic Data Centre via www.ccdc.cam.ac.uk/data_request/cif.

Computational details: All calculations were carried out with DFT^[31] as implemented in the Jaguar 7.0 suite^[32] of quantum chemistry programs. The spin-unrestricted (UDFT) approach was used in all cases. Geometry optimizations were performed with the PWPW91^[33] and the 6-31G** basis sets with Ni and Zn represented by using the Los Alamos LACVP basis that includes relativistic, effective, core potential.^[34] The energies were reevaluated by additional single-point calculations at each optimized geometry with Dunning's^[35] correlation consistent triple- ζ basis set cc-pVTZ(-f) with the standard double set of polarization functions. For metals, we used a modified version of LACVP, designed as LACV3P, in which the exponents were decontracted to match the effective core potential with triple- ζ quality. Vibrational-frequency calculations were done at the PWPW91/6-31G** level of theory to confirm proper convergence to minima and saddle points for equilibrium and transition-state geometries, respectively, and to derive the zero-point-energy (ZPE) and entropy corrections at room temperature. Solvation energies were evaluated by a self-consistent reaction field (SCRFF)^[36] approach based on accurate numerical solutions of the Poisson–Boltzmann equation.^[37] Solvation calculations were carried out at the gas-phase geometry by using 6-31G**/PWPW91 theory and employing a dielectric constant of $\epsilon=2.13$ for toluene. To obtain open-shell, broken-symmetry, singlet solutions is difficult and manual adjustments to the initial-guess wave function were often

necessary to converge to a plausible open-shell state and this was monitored by carefully analyzing the computed MSDs and the MOs.

The energy components were calculated following the standard protocol. The change in free energy in solution $\Delta G(\text{sol})$ was calculated as follows:

$$\Delta G(\text{sol}) = \Delta G(\text{gas}) + \Delta \Delta G_{\text{solv}} \quad (1)$$

$$\Delta G(\text{gas}) = \Delta H(\text{gas}) - T\Delta S(\text{gas}) \quad (2)$$

$$\Delta H(\text{gas}) = \Delta E(\text{SCF}) + \Delta \text{ZPE} \quad (3)$$

$\Delta G(\text{gas})$ is gas-phase Gibbs free-energy change, $\Delta \Delta G_{\text{solv}}$ is free energy of solvation difference as calculated with the continuum solvation model. The entropy of the solvent is implicitly included in the dielectric continuum model as the cavitation energy. $\Delta S(\text{gas})$ is gas-phase entropy change of the solute. $\Delta H(\text{gas})$ is gas-phase enthalpy change, $\Delta E(\text{SCF})$ is electronic energy change as computed from the SCF procedure, ΔZPE is zero-point energy correction difference and T is the temperature (298.15 K).

Acknowledgements

The generous support of the National Science Foundation (CHE-0956447, 0645381, 1001589), the Research Corporation (Cottrell and Scialog Awards to MHB) is gratefully acknowledged. LJKB thanks the Graduate Assistance in Areas of National Need program, Indiana University College of Arts and Sciences and Department of Chemistry fellowship programs, and Richard L. Lord for many helpful discussions.

- [1] a) R. Bonnett, B. D. Djelal, A. Nguyen, *J. Porphyrins Phthalocyanines* **2001**, 5, 652; b) D. E. J. G. J. Dolmans, D. Fukumura, R. K. Jain, *Nat. Rev. Cancer* **2003**, 3, 380; c) R. Bonnett, G. Martinez, *Tetrahedron* **2001**, 57, 9513.
- [2] a) S. G. DiMaggio, V. S. Y. Lin, M. J. Therien, *J. Org. Chem.* **1993**, 58, 5983; b) H. T. Uyeda, Y. Zhao, K. Wostyn, I. Asselberghs, K. Clays, A. Persoons, M. J. Therien, *J. Am. Chem. Soc.* **2002**, 124, 13806; c) Y.-P. An, Z. Yang, M. A. Ratner, *J. Chem. Phys.* **2011**, 135, 044706/1; d) N. Bennett, G. Xu, L. J. Esdaile, H. L. Anderson, J. E. MacDonald, M. Elliott, *Small* **2010**, 6, 2604; e) R. Charvet, K. Ariga, J. P. Hill, Q. Ji, A. H. Khan, S. Acharya, *Chem. Commun.* **2011**, 47, 6825; f) V. Gandhi, M. L. Thompson, T. D. Lash, *Tetrahedron* **2010**, 66, 1787; g) M. Koepf, J. Conradt, J. Szymkowski, J. A. Wytko, L. Allouche, H. Kalt, T. S. Balaban, J. Weiss, *Inorg. Chem.* **2011**, 50, 6073; h) F. Malvolti, P. Le Maux, L. Toupet, M. E. Smith, W. Y. Man, P. J. Low, E. Galardon, G. Simonneau, F. Paul, *Inorg. Chem.* **2010**, 49, 9101; i) G. Sedghi, V. M. Garcia-Suarez, L. J. Esdaile, H. L. Anderson, C. J. Lambert, S. Martin, D. Bethell, S. J. Higgins, M. Elliott, N. Bennett, J. E. Macdonald, R. J. Nichols, *Nature Nanotechnology* **2011**, 6, 517.
- [3] a) A. Osuka, H. Shimidzu, *Angew. Chem.* **1997**, 109, 93; *Angew. Chem. Int. Ed. Engl.* **1997**, 36, 135; b) J. D. Spence, T. D. Lash, *J. Org. Chem.* **2000**, 65, 1530; c) A. K. Sahoo, S. Mori, H. Shinokubo, A. Osuka, *Angew. Chem.* **2006**, 118, 8140; *Angew. Chem. Int. Ed.* **2006**, 45, 7972.
- [4] a) A. N. Cammidge, P. J. Scaife, G. Berber, D. L. Hughes, *Org. Lett.* **2005**, 7, 3413; b) K. Kurotobi, K. S. Kim, S. B. Noh, D. Kim, A. Osuka, *Angew. Chem.* **2006**, 118, 4048; *Angew. Chem. Int. Ed.* **2006**, 45, 3944; c) N. K. S. Davis, M. Pawlicki, H. L. Anderson, *Org. Lett.* **2008**, 10, 3945; d) S. Hayashi, M. Tanaka, H. Hayashi, S. Eu, T. Umeyama, Y. Matano, Y. Araki, H. Imahori, *J. Phys. Chem. C* **2008**, 112, 15576.
- [5] a) Y. Song, R. E. Haddad, S.-L. Jia, S. Hok, M. M. Olmstead, D. J. Nurco, N. E. Schore, J. Zhang, J.-G. Ma, K. M. Smith, S. Gazeau, J. Pecaut, J.-C. Marchon, C. J. Medforth, J. A. Shelnut, *J. Am. Chem. Soc.* **2005**, 127, 1179; b) C. J. Medforth, M. O. Senge, K. M. Smith, L. D. Sparks, J. A. Shelnut, *J. Am. Chem. Soc.* **1992**, 114, 9859;

- c) J. A. Shelnut, X.-Z. Song, J.-G. Ma, S.-L. Jia, W. Jentzen, C. J. Medforth, *Chem. Soc. Rev.* **1998**, 27, 31; d) R. E. Haddad, S. Gazeau, J. Pecaut, J.-C. Marchon, C. J. Medforth, J. A. Shelnut, *J. Am. Chem. Soc.* **2003**, 125, 1253; e) S. G. DiMagno, A. K. Wertsching, C. R. Ross II, *J. Am. Chem. Soc.* **1995**, 117, 8279; f) L.-M. Jin, L. Chen, J.-J. Yin, J.-M. Zhou, C.-C. Guo, Q.-Y. Chen, *J. Org. Chem.* **2006**, 71, 527; g) M.-S. Liao, T. Kar, S. M. Gorun, S. Scheiner, *Inorg. Chem.* **2004**, 43, 7151; h) J. Mack, Y. Asano, N. Kobayashi, M. J. Stillman, *J. Am. Chem. Soc.* **2005**, 127, 17697; i) K. E. Thomas, I. H. Wasbotten, A. Ghosh, *Inorg. Chem.* **2008**, 47, 10469.
- [6] a) H. Imahori, T. Umeyama, S. Ito, *Acc. Chem. Res.* **2009**, 42, 1809; b) N. K. S. Davis, A. L. Thompson, H. L. Anderson, *Org. Lett.* **2010**, 12, 2124; c) N. K. S. Davis, A. L. Thompson, H. L. Anderson, *J. Am. Chem. Soc.* **2011**, 133, 30.
- [7] H. Aihara, L. Jaquinod, D. J. Nurco, K. M. Smith, *Angew. Chem.* **2001**, 113, 3547; *Angew. Chem. Int. Ed.* **2001**, 40, 3439.
- [8] a) R. R. Jones, R. G. Bergman, *J. Am. Chem. Soc.* **1972**, 94, 660; b) R. G. Bergman, *Acc. Chem. Res.* **1973**, 6, 25; c) B. H. Long, J. Golik, S. Forenza, B. Ward, R. Rehffuss, J. C. Dabrowiak, J. J. Catino, S. T. Musial, K. W. Brookshire, T. W. Doyle, *Proc. Natl. Acad. Sci. USA* **1989**, 86, 2.
- [9] a) M. Nath, J. C. Huffman, J. M. Zaleski, *J. Am. Chem. Soc.* **2003**, 125, 11484; b) M. Nath, M. Pink, J. M. Zaleski, *J. Am. Chem. Soc.* **2005**, 127, 478.
- [10] a) M. Prall, A. Wittkopp, A. A. Fokin, P. R. Schreiner, *J. Comput. Chem.* **2001**, 22, 1605; b) P. R. Schreiner, *J. Am. Chem. Soc.* **1998**, 120, 4184.
- [11] J. D. Spence, E. D. Cline, D. M. Llagostera, P. S. O'Toole, *Chem. Commun.* **2004**, 180.
- [12] a) H.-K. Chang, S. Datta, A. Das, A. Odedra, R.-S. Liu, *Angew. Chem.* **2007**, 119, 4828; *Angew. Chem. Int. Ed.* **2007**, 46, 4744; b) X. Han, Y. Zhang, K. K. Wang, *J. Org. Chem.* **2005**, 70, 2406; c) P. R. Schreiner, M. Prall, V. Lutz, *Angew. Chem.* **2003**, 115, 5935; *Angew. Chem. Int. Ed.* **2003**, 42, 5757; d) Y. Yamamoto, A. Nagata, H. Nagata, Y. Ando, Y. Arikawa, K. Tatsumi, K. Itoh, *Chem. Eur. J.* **2003**, 9, 2469; e) I. V. Alabugin, K. Gilmore, S. Patil, M. Manoharan, S. V. Kovalenko, R. J. Clark, I. Ghiviriga, *J. Am. Chem. Soc.* **2008**, 130, 11535.
- [13] T. Chandra, B. J. Kraft, J. C. Huffman, J. M. Zaleski, *Inorg. Chem.* **2003**, 42, 5158.
- [14] a) D. W. Smith, Jr., H. V. Shah, K. P. U. Perera, M. W. Perpall, D. A. Babb, S. J. Martin, *Adv. Funct. Mater.* **2007**, 17, 1237; b) X. Cheng, J. Ma, J. Zhi, X. Yang, A. Hu, *Macromolecules* **2010**, 43, 909.
- [15] A. D. Adler, F. R. Longo, J. D. Finarelli, J. Goldmacher, J. Assour, L. Korsakoff, *J. Org. Chem.* **1967**, 32, 476.
- [16] M. J. Crossley, P. L. Burn, S. S. Chew, F. B. Cuttance, I. A. Newsom, *J. Chem. Soc. Chem. Commun.* **1991**, 1564.
- [17] a) B. P. Warner, S. P. Millar, R. D. Broene, S. L. Buchwald, *Science* **1995**, 269, 814; b) K. C. Nicolaou, Y. P. Hong, W. M. Dai, Z. J. Zeng, W. Wrasidlo, *J. Chem. Soc. Chem. Commun.* **1992**, 1542.
- [18] a) M. Prall, A. Wittkopp, P. R. Schreiner, *J. Phys. Chem. A* **2001**, 105, 9265; b) M. Nath, J. C. Huffman, J. M. Zaleski, *Chem. Commun.* **2003**, 858.
- [19] J. D. Rule, S. R. Wilson, J. S. Moore, *J. Am. Chem. Soc.* **2003**, 125, 12992.
- [20] a) L. D. Sparks, C. J. Medforth, M. S. Park, J. R. Chamberlain, M. R. Ondrias, M. O. Senge, K. M. Smith, J. A. Shelnut, *J. Am. Chem. Soc.* **1993**, 115, 581; b) M. O. Senge, *Chem. Commun.* **2006**, 243.
- [21] a) K. M. Barkigia, M. W. Renner, L. R. Furenliid, C. J. Medforth, K. M. Smith, J. Fajer, *J. Am. Chem. Soc.* **1993**, 115, 3627; b) W. W. Kalisch, M. O. Senge, *Angew. Chem.* **1998**, 110, 1156; *Angew. Chem. Int. Ed.* **1998**, 37, 1107; c) D. J. Nurco, C. J. Medforth, T. P. Forsyth, M. M. Olmstead, K. M. Smith, *J. Am. Chem. Soc.* **1996**, 118, 10918; d) M. O. Senge, I. Bischoff, *Eur. J. Org. Chem.* **2001**, 1735; e) M. O. Senge, W. W. Kalisch, *Inorg. Chem.* **1997**, 36, 6103; f) M. O. Senge, M. W. Renner, W. W. Kalisch, J. Fajer, *J. Chem. Soc., Dalton Trans.* **2000**, 381.
- [22] a) P. Bhyrappa, C. Arunkumar, B. Varghese, *Inorg. Chem.* **2009**, 48, 3954; b) P. Bhyrappa, M. Sankar, B. Varghese, *Inorg. Chem.* **2006**, 45, 4136; c) M. O. Senge, T. Ema, K. M. Smith, *J. Chem. Soc. Chem. Commun.* **1995**, 733.
- [23] M. Gouterman in *The Porphyrins, Vol. 3* (Ed.: D. Dolphin), Academic Press, New York, **1978**.
- [24] a) M. Gouterman, G. Wagniere, L. C. Snyder, *J. Mol. Spectrosc.* **1963**, 11, 108; b) E. J. Baerends, G. Ricciardi, A. Rosa, S. J. A. van Gisbergen, *Coord. Chem. Rev.* **2002**, 230, 5.
- [25] Porphyrins that underwent cyclization required corrections for mass balance, due to the fact that the cyclization of each enediyne results in a net loss of two H atoms. Also taken under consideration was the source of the H atoms and the overall entropy gain of the reactions therein. Corrections were made as suggested by Cramer (C. J. Cramer, *J. Am. Chem. Soc.* **1998**, 120, 6261), and were performed as follows. To energies of the starting enediyne **3** were added the calculated energies of two equivalents of CHD, a common H donor in Bergman cyclization reactions. This was repeated for compounds **3-TS** through **6**. Compound **7** was corrected with one equivalent of CHD and one equivalent of benzene, and compound **8** was corrected with one equivalent each of CHD, benzene, and H₂ molecules. Compounds **8-TS** through **11** were also corrected this way. Compound **12** was corrected with two equivalents of benzene and one equivalent H₂, whereas **13** was corrected with two equivalents each of benzene and H₂ molecules. This assured that the relative energies of all compounds could be directly compared to each other, because all had the same number of net atoms.
- [26] Although solid-state DSC temperatures (ca. 150°C) and cyclization reaction conditions in solution (80–155°C) seem incongruent with the initial Bergman cyclization barrier of 17.4 kcal mol⁻¹, reaction of **3a** at 40°C for 120 h generates 50% conversion and 10% isolated yield of product **8a**; this indicates that the calculated reaction barrier is indeed markedly lower than these optimal reaction temperatures imply.
- [27] Experimental thermal Bergman cyclization of **3** to **8** is typically performed anaerobically, with isolation and purification conducted aerobically. Under these conditions, **8** is presumed to be formed via tetrahydro species **7**, which subsequently converts to **8** either through loss of H₂ (anaerobically) or oxidation by O₂ (aerobically). Thermodynamically, loss of 2H₂ is downhill by 45 kcal mol⁻¹, and control reactions with anaerobic analyses illustrate distinct formation of a piconoporphyrin product. Additionally, computation of the reaction of **7** + O₂ → **8** + 2H₂O is downhill by about 145 kcal mol⁻¹. Whereas oxidation-assisted formation of the piconoporphyrin product is clearly favored and has been demonstrated at ambient temperature by using external addition of 2,3-dichloro-5,6-dicyano-1,4-benzoquinone (DDQ; M. Nath, J. C. Huffman, J. M. Zaleski, *Chem. Commun.* **2003**, 858a), the H₂ evolution pathway is the most fundamental of viable reaction trajectories.
- [28] C. J. Cramer, *J. Am. Chem. Soc.* **1998**, 120, 6261.
- [29] I. Alabugin, B. Breiner, M. Manoharan, *Adv. Phys. Org. Chem.* **2007**, 42, 1.
- [30] G. Stork, A. Brizzolara, H. Landesman, J. Szmuszkovicz, R. Terrell, *J. Am. Chem. Soc.* **1963**, 85, 207.
- [31] a) R. G. Parr, W. Yang, *Density-Functional Theory of Atoms and Molecules*, Oxford University Press, New York, **1989**; b) T. Ziegler, *Chem. Rev.* **1991**, 91, 651.
- [32] Jaguar 7.0, Schrödinger, LLC, New York, NY, 2007.
- [33] a) J. C. Slater, *Quantum Theory of Molecules and Solids, Vol. 4: The Self-Consistent Field for Molecules and Solids*, McGraw-Hill, New York, **1974**; b) J. P. Perdew, *Electronic Structure of Solids*, Akademie Verlag, Berlin, **1991**; c) J. P. Perdew, Y. Wang, *Phys. Rev. B* **1992**, 45, 13244.
- [34] P. J. Hay, W. R. Wadt, *J. Chem. Phys.* **1985**, 82, 299.
- [35] T. H. Dunning, *J. Chem. Phys.* **1989**, 90, 1007.
- [36] a) J. Tomasi, M. Persico, *Chem. Rev.* **1994**, 94, 2027; b) C. J. Cramer, D. G. Truhlar, *Structure and Reactivity in Aqueous Solution, ACS Symposium Series 568*, American Chemical Society, Washington, D. C., **1994**; c) C. J. Cramer, D. G. Truhlar, *Chem. Rev.* **1999**, 99, 2161.

[37] a) D. J. Tannor, B. Marten, R. Murphy, R. A. Friesner, D. Sitkoff, A. Nicholls, B. Honig, M. Ringnalda, W. A. Goddard, III, *J. Am. Chem. Soc.* **1994**, *116*, 11875; b) B. Marten, K. Kim, C. Cortis, R. A.

Friesner, R. B. Murphy, M. N. Ringnalda, D. Sitkoff, B. Honig, *J. Phys. Chem.* **1996**, *100*, 11775.

Received: August 10, 2011
Published online: November 14, 2011